*Aerosol and Air Quality Research*, 14: 1799–1811, 2014

ISSN: 1680-8584 print / 2071-1409 online
doi: 10.4209/aaqr.2014.08.0165

# Identification of Missing Anthropogenic Emission Sources in Russia: Implication for Modeling Arctic Haze

**Kan Huang[1], Joshua S. Fu[1*], Elke L. Hodson[2†], Xinyi Dong[1], Joe Cresko[2], Vitaly Y. Prikhodko[3], John M. Storey[3], Meng-Dawn Cheng[3]**

[1] *Department of Civil and Environmental Engineering, The University of Tennessee, Knoxville, TN 37996, USA*
[2] *U.S. Department of Energy, Washington, DC, USA*
[3] *Energy and Environmental Sciences Directorate, Oak Ridge National Laboratory, Oak Ridge, TN, USA*

## ABSTRACT

Any comprehensive simulation of air pollution in the Arctic requires an accurate emission inventory. Using a community global emission inventory EDGAR v4.2 (Emissions Database for Global Atmospheric Research), GEOS-Chem modeling underestimated aerosol optical depth by 150–300% when compared to ground-based sites in Russia. Emissions from power plants, gas flaring, and mining were found significantly underestimated or even missing in EDGAR's Russian emission inventory. Approximately 70% of Russian provinces had lower $NO_x$ and $PM_{10}$ emission from power plants in EDGAR as compared to a Russian federal emission inventory. Emissions from gas flaring dominated in Russia's main oil and gas producing regions. However, it is completely missing in EDGAR. In addition, EDGAR underestimated Russia's mining emissions in most of its remote areas. Overall, we find EDGAR underestimated Russia's emissions especially at high latitudes and this could overlook the impact of Russian emissions on the Arctic if EDGAR is used as input for models.

***Keywords:*** Russia; EDAGR; Emission underestimation; Arctic.

## INTRODUCTION

The Arctic region is vulnerable to the transport and deposition of particulate matter (PM), such as black carbon, and sulfate. The Arctic Circle (north of 66°33′44″N) includes parts of Alaska, Europe and vast regions of Canada and Russia. Anthropogenic emissions and biomass burning originating from these countries have been shown to be the main cause of Arctic haze (Law and Stohl, 2007). Most of the Arctic region countries have relatively reliable emission inventories except Russia due to the difficulties of quantifying the local emission factors and locating emission sources. Results from trajectory models (e.g., FLEXPART (Hirdman *et al.*, 2010a, b), WRF (Harrigan *et al.*, 2011), HYSPLIT (Huang *et al.*, 2010), PSCF (Eleftheriadis *et al.*, 2009), and Canadian Meteorological Centre model (Sharma *et al.*, 2006)), concluded that northern and central Russia was the major source region contributing to Arctic haze. The former USSR contributed to the haze measured at a Canadian high Arctic site with the dominant fraction of 67% during a 16-year period, followed by the European Union (18%) and North America (15%) (Huang *et al.*, 2010). Meanwhile, the contribution from Asia or Southeast Asia was negligible (Stohl, 2006; Hirdman *et al.*, 2010b).

Recent 3-D chemical transport modeling efforts, however, have shown contrasting and inconsistent results. For instance, Asian anthropogenic emissions were suggested to be the dominant source of Arctic CO pollution by using GEOS-Chem (Fisher *et al.*, 2010). A GISS model (ModelE) study also suggested that south Asia (industrial and biofuel emissions) and biomass burning were the predominant sources of Arctic soot (Koch and Hansen, 2005). A multi-model (17 models) research effort determined that the European emissions dominated at the surface of Arctic but East Asian emissions were more dominant in the upper troposphere (Shindell *et al.*, 2008). Models generally underpredicted black carbon concentrations in the Arctic (Koch and Hansen, 2005; Shindell *et al.*, 2008), and the largest divergence in model results occurred in northern Eurasia and the remote Arctic from the AeroCom model inter-comparison (Koch *et al.*, 2009). For the latter study, anthropogenic emissions from Russia and Asia had to be doubled to match with the observations (Wang *et al.*, 2011). Recently, Stohl *et al.* (2013) used a Lagrangian particle dispersion model FLEXPART to greatly improve the simulated black carbon over the Arctic by using daily-

† Oak Ridge Institute for Science and Education Fellow

* Corresponding author.
Tel.: 1-865-974-2503; Fax: 1-865-974-2669
*E-mail address:* jsfu@utk.edu

varying residential combustion emissions and introducing a global gas flaring emission inventory. Lacking of certain emission sources and improper treatment of emission temporal profiles are pointed out against previous studies of ascribing unsatisfactory model performances to physical process problems in aerosol models.

In this study, we aim to identify several underestimated and missing emission sources in the Russian part of the global emission inventory EDGAR, with a specific focus on the energy, gas flaring and mining sectors. Model simulation using EDGAR was evaluated against observations in Russia. Large point sources (i.e., thermal power plants) in EDGAR were compared to a global power plant database CARMA and satellite detection of $NO_2$ columns. Gas flaring areas were retrieved from satellite imagery and the emissions from gas flaring were estimated. This study first demonstrated the differences of multiple emission sectors between EDGAR and a Russian federal emission inventory. It should be noted that this study doesn't aim to demonstrate how the identified gaps between various emission databases will translate into modeling results, but draw conclusions on the importance of improving the Russian emission inventory on modeling the origin and impact of the Arctic haze.

## METHODS

EDGAR was first used to determine whether using this emission dataset as input to transport modeling would represent measured concentrations of pollutants. Then, other data sets, including a database of power plants, an emission inventory from the Russian federal government, and data on gas flaring were utilized to verify possible underestimated or missing emission sectors investigated in this study.

### *Emission Data*

*EDGAR Global Emission Inventory*

EDGAR is a global database for anthropogenic emissions of greenhouse gases and air pollutants with a spatial resolution as fine as 0.1° × 0.1°. Sectoral emissions are available, including energy production, transportation, industries, residential, and biomass burning. Biomass burning emissions are based on the Global Fire Emissions Database (GFED). It is generated on the monthly basis (van der Werf *et al.*, 2010) with temporal scaling profiles of daily and 3-hourly (Mu *et al.*, 2010). Conversions from carbon emissions to various species are based on emission factors from Andreae and Merlet (2001). The methodology for the EDGAR emission calculations is well established (EDGAR, 2013). It has been used as a default emission inventory for various models, e.g., GEOS-Chem, MOZART, the unified EMEP model, ECHAM5-HAMMOZ, GISS-PUCCINI, etc. We used the newest version of EDGAR, v4.2, and the most recent year available, which is 2008. However, due to the lack of up-to-date local activity data, emissions estimates in recent years are not necessarily reliable for Russia. For instance, compared to EDGAR v4.1, the corrections of power plant emissions were only made for sources in China (EDGAR, 2011). In this study, we make a distinction between the global EDGAR database, which we use as input for the global chemical transport model GEOS-CHEM and the Russian part of the EDGAR database, which we compare to various other databases (hereinafter called "RUS_EDGAR").

*Russian Federal Emission Inventory*

The Russian Federal State Statistics Service (FSSS, http://www.gks.ru) provides its national emissions inventory (hereinafter called "RUS_FSSS") of air pollutants for a limited range of emission sectors. RUS_FSSS inventory data is available for fossil-fuel fired power plants and mining, but not gas flaring. We compared 2008 data from RUS_FSSS to be consistent with RUS_EDGAR. The pollutants reported by FSSS, include solid particles, carbon monoxide, nitrogen oxides, and hydrocarbons. The methodologies for estimating the pollutant emissions were established by various Russian research institutes. A list of the approved emission calculation methodologies currently in use by the Russian Federation are documented by SRI-Atmosphere (SRI Atmosphere, 2012). The emission of a specific air pollutant into the atmosphere is estimated by using the following equation:

$$M_i = \sum(M_{raw,i} \times (1 - \eta_i)), \quad (1)$$

where $i$ represents a specific economic sector; $M_{raw,i}$ is the annual total raw emission of sector $i$ prior to technology controls; $\eta_i$ is the removal efficiency of sector $i$; and $M_i$ is the annual total emission released into the atmosphere. To convert the RUS_FSSS total suspended particulate (TSP) emission data to the more commonly used metric of particulate matter with a diameter of 10 μm or less ($PM_{10}$), we multiplied the original RUS_FSSS TSP data by a scale factor of 0.675, which was calculated based on an average over multiple estimates of emission factors for $PM_{10}$ and TSP from coal combustion in power plants (EEA, 2013). Table 1 shows these calculated nationwide emissions of $PM_{10}$, and reported $NO_x$ and CO, for the power and mining sectors in the Russian Federation, from FSSS for 2008. In order to allocate the nationwide emissions to the provincial level, we used the same relative provincial distribution of the Russian category entitled "social-economic indicators" (FSSS, 2011) to allocate national emissions by province. This is equivalent to:

$$M_{i,k} = M_i \times (E_{i,k}/\sum E_{i,k}), \quad (2)$$

where $k$ represents a specific Russian province; $E_{i,k}$ is the annual revenues rendered in sector $i$ in province $k$ (unit: million rubles); And $M_{i,k}$ is the annual emission in sector $i$ in province $k$.

### *CARMA – A Global Power Plant Dataset*

Carbon Monitoring for Action (CARMA) is a database under the operation of the Confronting Climate Change Initiative at the Center for Global Development (http://www.carma.org). It contains information about the energy production, intensity, carbon emission and locations of the power plants worldwide. CARMA compiles data from both national publicly disclosed databases and a commercial database of the world's power plants (Wheeler and Ummel,

**Table 1.** 2008 Russian emission of $PM_{10}$, $NO_x$ and CO (units: Gg) for the energy industry and mining sectors (with sub-sectors) based on FSSS.

| Sector | $PM_{10}$ | $NO_x$ | CO |
|---|---|---|---|
| **Energy Industry** | 830.67 | 3418.85 | 637.81 |
| Electricity production | 588.69 | 2814.96 | 164.58 |
| Transmission and distriction of steam and hot water | 228.23 | 591.51 | 454.87 |
| Collection, purification and distribution of water | 5.92 | 10.14 | 17.25 |
| **Mining** | 275 | 151.47 | 2229.09 |
| Mining of coal | 37.62 | 13.35 | 45.25 |
| Production of crude oil and natural gas | 150.09 | 99.83 | 2043.8 |
| Mining of metal ores | 52.05 | 27.43 | 128.28 |
| Other mining and quarrying | 30.81 | 8.96 | 10.91 |

2008). CARMA v2.0 reports energy data for the year 2000, 2007, and projections for future years after 2007 based on planned construction and retirements. The total energy production of power plants in Russia from CARMA was 931 billion kWh, close to that of 962 billion kWh reported from the U.S. Energy Information Administration (EIA, 2013). For the analysis presented in this study, we use data from 2007, the most recent year of historical data in the CARMA database.

### *Gas Flaring Dataset*

National and global gas flaring volumes are estimated based on satellite sensor observations from the U.S. Air Force Defense Meteorological Satellite Program (DMSP) Operational Linescan System (OLS). NOAA NGDC (National Geophysical Data Center) serves as the long-term archive for DMSP (http://www.ngdc.noaa.gov/dmsp/interest/gas_flares.html). Gas flaring activity is detected from the visible band signal at night and identified based on a parameter called "lights index". More detailed descriptions of the methodology can be found in (Elvidge *et al.*, 2009).

### *GEOS-Chem Simulation and Model Evaluation*

A 3-D global chemistry model GEOS-Chem (v8-02-03) was used to evaluate the reliability of RUS_EDGAR in this study. The model is driven by GEOS-5 (Goddard Earth Observing System) assimilated meteorological inputs from the NASA Global Modeling and Assimilation Office (GMAO) for 2008. The model's resolution is set at 2 by 2.5 degrees with 47 vertical layers. The global anthropogenic emission input to the model is from EDGAR, superseded by regional emission inventories, including the NASA INTEX-B inventory for South and East Asia, the EMEP inventory for Europe, the BRAVO inventory for Mexico, and the USEPA's NEI for the US. The emission inventory for the rest of the world is from EDGAR v4.2.

The model performances of GEOS-Chem have been intensively evaluated in the United States (Fu *et al.*, 2011; Zhang *et al.*, 2012) and East Asia (Lin, 2012), suggesting its applicability for simulating global air pollution transport and transformation given reliable emission inventory. Currently, limited model simulations have been conducted for Russia (Makarova *et al.*, 2011). To evaluate the GEOS-Chem model performance in Russia, AERONET (Aerosol Robotic NETwork, (Holben *et al.*, 1998)) observations were used as they are the only available publicly accessed aerometric network in Russia with assured quality. In 2008, data from five AERONET sites were available. These sites in Russia are shown in Fig. 1, including Moscow, Yekaterinburg, Tomsk, Irkutsk, and Yakutsk. Aerosol optical depth (AOD) at the visible wavelength of 500nm was chosen as the parameter for the model evaluation. The method of converting modeled aerosol chemical species to AOD is described in (Fu *et al.*, 2012; Huang *et al.*, 2012).

### *OMI $NO_2$ Column Concentrations*

In this study, the $NO_2$ columns retrieved from the Ozone Monitoring Instrument (OMI) is used to verify the locations of large point sources. The capability of detecting large point emission sources by using the OMI satellite retrieves have been well demonstrated (Zhang *et al.*, 2009; Li *et al.*, 2010). OMI is a nadir-viewing near-UV/Visible spectrometer aboard NASA's Earth Observing System's (EOS) Aura satellite. It can measure the sunlight at a spectral region of 264–504 nm with a spectral resolution between 0.42 nm and 0.63 nm and a nominal ground footprint of $13 \times 24$ km$^2$ at nadir. In this study, the $NO_2$ column concentrations are from the OMI Level 3 daily global products with a spatial resolution of $0.25° \times 0.25°$. Spring data are used as higher pollutant concentrations occur during the cold season compared to the warm season. In addition, the satellite had very limited coverage over the high latitudinal regions of Russia from late autumn to winter due to the low solar zenith angles.

## RESULTS AND DISCUSSION

### *Underestimated Russian Emission from Perspective of Modeling*

The comparisons between GEOS-Chem modeled AOD by utilizing EDGAR and the observed AOD at the five Russian AERONET sites are shown in Fig. 2. The left panels show the temporal variations (shown in Julian days) and the right panels represent the scatter plots between observation and simulation. Significant discrepancies between the observed and modeled AOD are evident. As shown in the left panels of Fig. 2, the model predicted relatively flat temporal variations and missed almost all the peaks. Modeled and observed AOD differed by a factor of 5–10 during intensive pollution episodes. Observed AOD peaked at different times depending

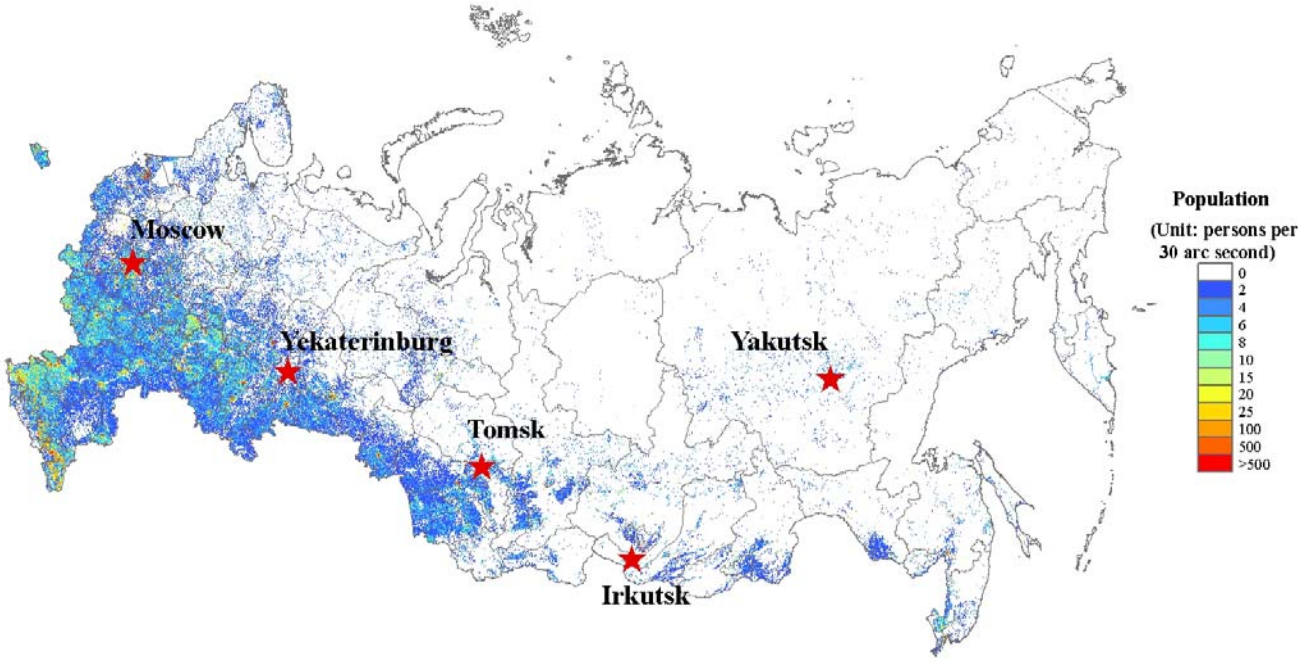


**Fig. 1.** Population density of Russia with a grid spacing of 30-arc seconds (approximately 1 kilometer). Red stars represent the five AERONET sites set up in Russia, i.e., Moscow, Yekaterinburg, Tomsk, Irkutsk, and Yakutsk.

on the site locations, possibly due to the variations of local emission intensities and local meteorology. Biomass burning was investigated to be insignificant for the high AOD events by conducting sensitivity simulation with zeroing out emissions from biomass burning. Lowest biomass burning emissions in this study year (2008) during the 2000s should be responsible for this (Fig. S1). Overall, neither peak episodes or the spatial differences of AOD could be reproduced by the model at all. Fig. 2 (right panels) showed evidence that AOD at all sites in Russia were significantly underestimated by the model. AOD were biased low by about 2–3 folds for Moscow and Yekaterinburg, two of the biggest cities in Russia. In some smaller cities (e.g., Tomsk and Irkutsk) and remote areas (e.g. Yakutsk), AOD were underestimated by about 1.5–2 folds. As stated earlier, GEOS-Chem performed relatively well in various regions, where emissions are relatively reliable. The unsatisfactory model performance in Russia strongly suggested that Russia's emissions in EDGAR (RUS_EDGAR) needs substantial improvement.

### *Emissions from Fossil-Fuel Fired Power Plants*

#### *Detection of Missing Power Plants in RUS_EDGAR from CARMA and OMI*

In this section, we compared CARMA and RUS_EDGAR to locate possible regions of Russia where the two databases differ in their co-locations of fossil-fuel fired power plants. The locations of fossil-fuel fired power plants in RUS_EDGAR (black squares) and CARMA (pink dots) for 2007 are shown in Fig. 3(a). In most areas, pink dots were surrounded by the squares, indicating that a power plant was identified in both databases. However, we found that CARMA contained more sites than RUS_EDGAR in some regions, e.g., the two sub-regions highlighted in Figs. 3(b) and 3(c).

To further evaluate the reliability of these "additional" fossil-fuel fired power plants from CARMA, the spatial distribution of $NO_2$ column concentrations observed from OMI during the spring of 2007 is overlaid in Fig. 3. As shown in Fig. 3(a), the areas where there were co-located fossil-fuel fired power plants from both RUS_EDGAR and CARMA generally showed high $NO_2$ concentrations. Emissions from electricity and heat production contributed 56% to the total $NO_x$ emissions in Russia according to RUS_FSSS. Specifically, we found that areas where there were additional fossil-fuel fired power plants in CARMA compared to RUS_EDGAR also showed high $NO_2$ column concentrations, further suggesting that there were indeed fossil-fuel fired power plants missing in EDGAR.

Two sub-regions with apparent missing power plants were selected for discussion as marked by the red rectangles in Fig. 3(a). Sub-regions 1 (Fig. 3(b)) refers to the Urals Federal District (which contains the Khanty-Mansiysk and Yamalo-Nenets Autonomous Okrugs) and Sub-regions 2 (Fig. 3(c)) refers to Chukotka Autonomous Okrug. The high $NO_2$ columns are likely not related to the regional/long-range transport, as the adjacent areas around these two regions were accompanied with relatively low $NO_2$ concentrations, hence suggesting local emission sources. Also, it is unlikely that residential emissions contributed significantly to the high $NO_2$ concentrations there, due to the fairly low population densities (fewer than 3 persons/km$^2$) in these areas as shown in Fig. 1.

Fig. 3(b) shows that a total of 16 fossil-fuel fired power plants (some power plants were closely located and couldn't be differentiated clearly in the figure) were missing in EDGAR over Sub-region 1. High $NO_2$ concentrations were

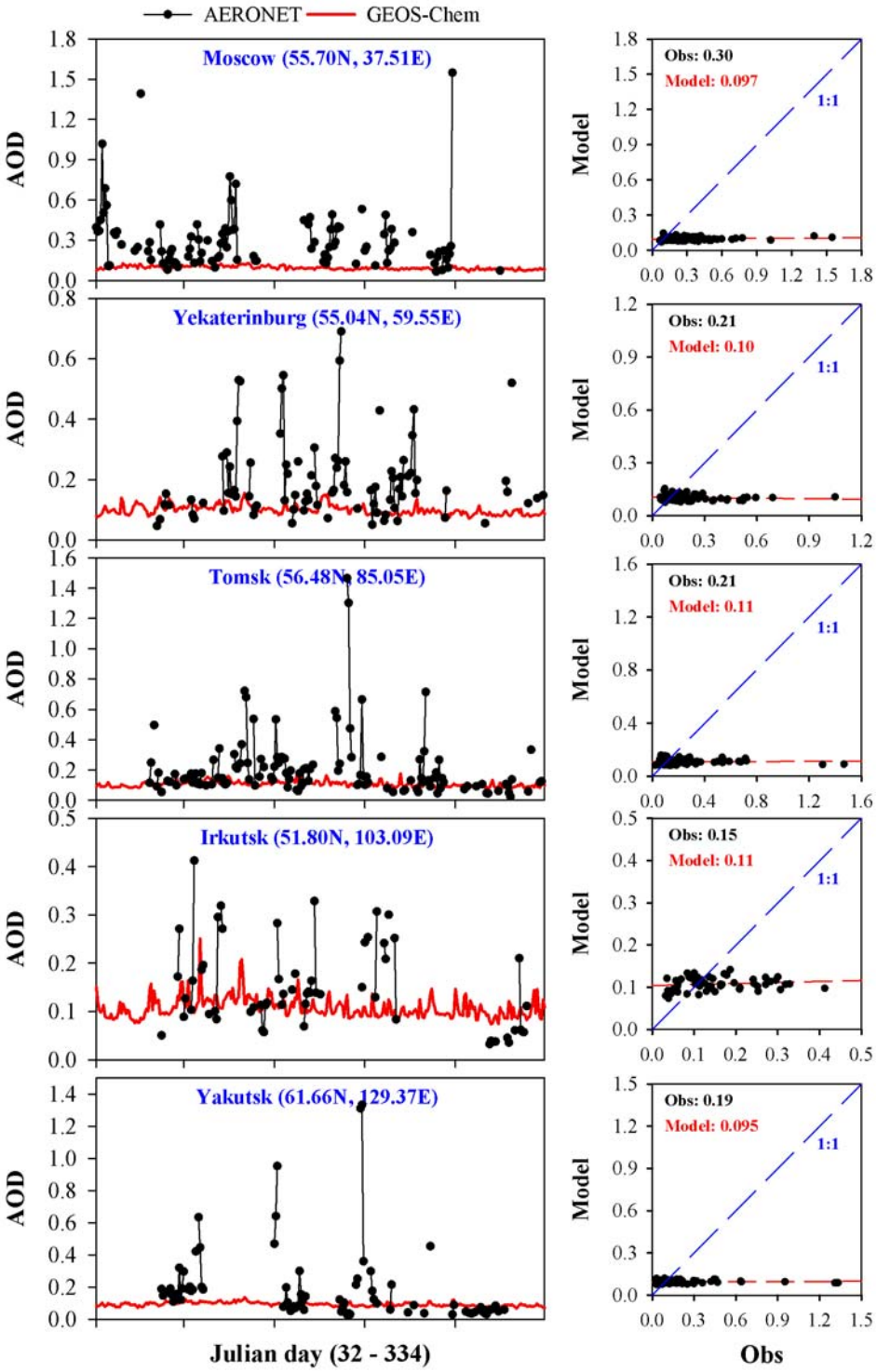


**Fig. 2.** Left panels: temporal variations of measured (black dots) Aerosol Optical Depth (AOD) and GEOS-Chem modeled (red lines) AOD at five AERONET sites in Russia for 2008. Right panels: Scatter plots of modeled vs. measured AOD. The red and blue dashed lines represent the regressions and the 1:1 lines forced through zero, respectively. The average AOD values of observation and model simulation appear to the top of the plots for each site.

observed around the areas where power plants were located, especially around co-located power plants. For instance, relatively high $NO_2$ column concentration of about 5.0–5.5 $\times$ $10^{15}$ molecules/cm$^2$ were observed around the P11-P15 power plants (Fig. S2 and Table S1). In the Khanty-Mansiysk Autonomous Okrug of the Urals Federal District (Fig. 3(b)), it was noted that one large capacity power plant (P13: SURGUT-2) was missing in RUS_EDGAR with its annual intensity of 1.56 $\times$ $10^7$ MWh based on CARMA. It ranked as the fifth largest fossil-fuel fired power plant in Russia.

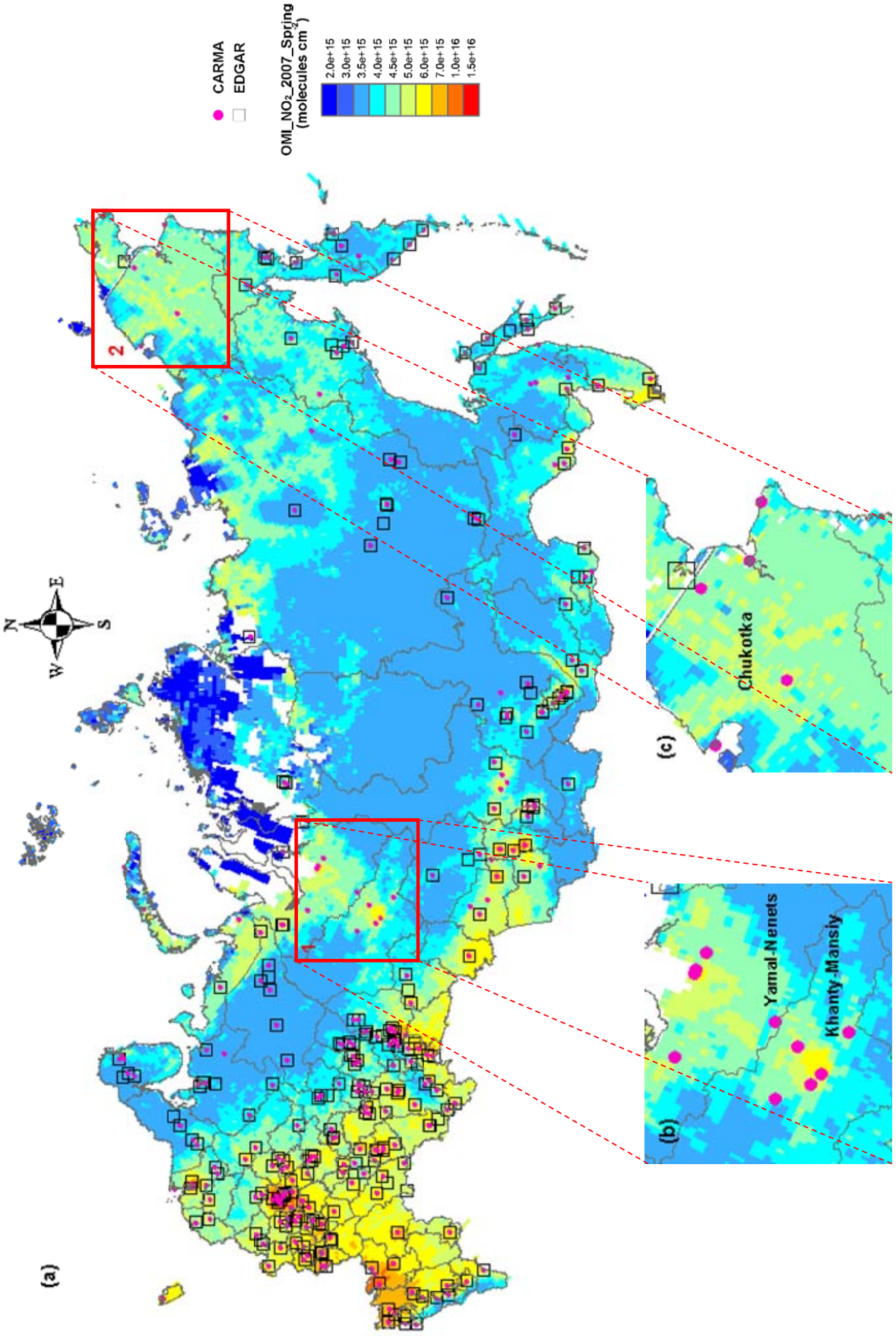


**Fig. 3.** 2007 Springtime average OMI $NO_2$ (0.25° × 0.25°) column concentrations (molecules/cm$^2$) over (a) the whole Russian country and two sub-regions, i.e., (b) Sub-regions 1: the Urals Federal District and (c) Sub-regions 2: Chukotka Autonomous Okrug. Pink dots and black squares represent the locations of thermal power plants from CARMA and EDGAR v4.2 in 2007, respectively. The CARMA power plant data is at precise locations while the EDGAR is grided with a spatial resolution of 0.1° × 0.1°.

Also, its fuel type was investigated to be fuel oil/diesel, which had high emission factors for pollutant gaseous (e.g., $NO_x$ and CO) and particulate matter. The total missing energy production in the Khanty-Mansiysk and Yamalo-Nenets Autonomous Okrugs reached $2.35 \times 10^7$ and $2.23 \times 10^6$ MWh based on CARMA, respectively, which could contribute significantly to the air pollutants emission. It is noted that Sub-region 1, specifically the Yamal-Nenets Autonomous Area, shows widely dispersed high $NO_2$ spots besides at locations near the missing fossil-fuel fired power plants. As discussed in Section 3.3, this is a region of significant gas flaring emissions. This explained the large scale high $NO_2$ zone in Sub-region 1.

Sub-region 2 is in the northeast part of the Chukotka Autonomous Okrug (Fig. 3(c)). Only one fossil-fuel fired power plant appeared in RUS_EDGAR, while there were five more power plants (P17–P21, Fig. S2) found in CARMA. The spatial distribution of $NO_2$ columns in Fig. 3(c) verified the existence of these plants. The total energy production of missing power plants in Sub-region 2 reached $5.19 \times 10^5$ MWh based on CARMA, which was about 400% higher than that in RUS_EDGAR. In addition to these two regions, there was also considerable absence of power plants distributed in other regions. Fig. S2 and Table S1 illustrate the locations and information of individual missing power plants. The total underestimated energy production in EDGAR as compared to CARMA reached $6.18 \times 10^7$ MWh (42% from coal-fired power plants), accounting for 9.6% of the total energy production in Russia. In other words, RUS_EDGAR underrepresented about 10% lower energy input, which could be significant when translating the country's energy inputs into emissions.

*Comparison of RUS_EDGAR to RUS_FSSS*

We further compared RUS_EDGAR and RUS_FSSS at the provincial level. Fig. 4 shows the scatter plot between the two emission inventories for $NO_x$ and $PM_{10}$ emissions from fossil-fuel fired power plants. Each scatter represents one Russian province. For $NO_x$ emissions (Fig. 4(a)), approximate one third of provinces were in relatively good agreement between the two datasets as indicated by the dots within the 1:2 and 2:1 lines. However, approximate two-thirds of provinces fell above the 2:1 line, indicating significant underestimation of RUS_EDGAR compared to RUS_FSSS. Khanty-Mansiysk Autonomous Okrug was the province that we found to be the most underestimated in RUS_EDGAR. Its $NO_x$ emissions from fossil-fuel fired power plants in RUS_FSSS reached 140.3 Gg, which ranked the third highest of any province within the Russian Federation. However, this source area was not even registered in RUS_EDGAR. In addition, $NO_x$ emissions from power plants in the Yamalo-Nenets and Chukotka Autonomous Okrugs were also lower in RUS_EDGAR compared to RUS_FSSS by a factor of ~30. This finding corroborated the results from the OMI observation that hot spots of $NO_2$ columns occurred in areas where many fossil-fuel fired power plants were missing in RUS_EDGAR.

Fig. 4(b) shows the comparison for $PM_{10}$ emission from fossil-fuel fired power plants between the two emission inventories. $PM_{10}$ emissions were even more underestimated than for $NO_x$. The total national $PM_{10}$ emission from fossil-fuel fired power plants was approximately 830 Gg in RUS_FSSS in 2008 (Table 1), about 2 times higher than that in RUS_EDGAR. The regional differences between the two databases in the distribution of $PM_{10}$ are similar to $NO_x$. In Section 3.1, we show that GEOS-Chem simulations, using EDGAR, significantly underestimated AOD for the five AOD measurement sites in Russia. The missing $PM_{10}$ and $NO_x$ emissions identified here likely explain part of the observed AOD underestimation.

***Emissions from Gas Flaring***

Gas flaring is a widely used practice for the disposal of associated gas in oil production and processing facilities

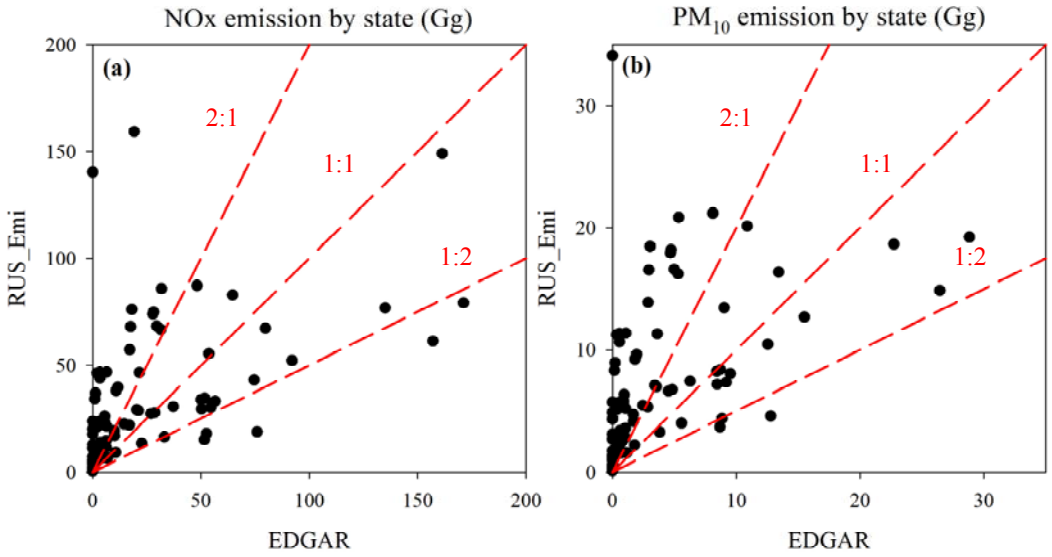


**Fig. 4.** Scatter plot between (a) $NO_x$ and (b) $PM_{10}$ emission from the new Russian emission inventory and the 2008 EDGAR emission inventory at a provincial scale. Dash lines represent the 2:1, 1:1, and 1:2 ratios.

where there is insufficient infrastructure for utilization of the gas. Flaring causes hazards to human health and also contributes to global anthropogenic emissions (McEwen and Johnson, 2012). Russia possesses the largest gas flaring volume in the world. In 2008, the amount of gas flaring from Russia reached about 42 BCM (billion cubic meters) and contributed 29% of total gas flared worldwide (World Bank, 2012). Although included in the EDGAR inventory, gas flaring emissions were estimated to be almost zero for Russia.

Fig. 5 shows the locations of gas flaring in Russia derived from the U.S. Air Force Defense Meteorological Satellite Program (DMSP) Operational Linescan System (OLS). Five major flaring areas are marked in the figure, of which, Khanty-Mansiysk Autonomous Okrug (① in Fig. 5) possessed the largest area of gas flaring. Khanty-Mansiysk produces 51% of Russia's oil and is Russia's largest oil producing region. The annual flaring volume from Khanty-Mansiysk Autonomous Okrug reached 20.0 BCM, which was 47.6% of the gas flared from the whole Russian Federation (NOAA, 2011). Assuming flared area is proportional to flared gas volume, Yamalo-Nenets Autonomous Okrug, Komi Republic, Nenets Autonomous Okrug, and Tomsk Oblast (②–⑤ in Fig. 5) were the other four largest regions that contributed to Russia's national flaring emission. Relatively low APG (Associated Petroleum Gas) utilization rates were the major reason for the large gas flaring emissions in these regions. For instance, the oil and gas fields in the Urals and Western Siberia (e.g., Khanty-Mansiysk Autonomous Okrug, Yamalo-Nenets Autonomous Okrug and Tomsk Oblast) only had a moderate APG utilization rate of 55–78% (FNI, 2010), and the oil and gas fields in the Northwestern Federal District (e.g., Komi Republic, Nenets Autonomous Okrug) had a APG utilization rate of only slightly above 35% (Knizhnikov and Poussenkova, 2009).

Table 3 shows the results of the 2008 emissions for $PM_{10}$, $NO_x$, and CO in the five major flaring regions and the whole Russian Federation based on the annual gas flaring volumes and emission factors. To estimate the emissions from flaring, we applied the mean emission factors (EFs) for $PM_{10}$, $NO_x$, and CO as listed in Table 2. The EFs in Table 2 have wide ranges and high uncertainties due to differences in fuel type, heating values, combustion efficiency, etc. (RTI International, 2011). We estimate the Russian national $PM_{10}$, $NO_x$, and CO emissions from gas flaring to be 132, 126, and 601 Gg, respectively. Compared to Russia's emissions from the energy industry at a national scale, the magnitudes of flaring emission were a factor of 8 and 26 lower for $PM_{10}$ and $NO_x$, respectively, because flaring occurred in a relatively limited geographic region in Russia (Fig. 5). National CO emissions from flaring were close to that from power plants, mainly due to incomplete combustion.

For the regions where flaring occurred, its emission dominated over other sources. For example, gas flaring emissions of $PM_{10}$, $NO_x$, and CO from Khanty-Mansiysk were 63, 60, and 286 Gg in 2008 as compared to those of 34, 26, and 140 Gg from the energy industry, respectively. In Yamalo-Nenets, gas flaring emissions were even more dominant with emissions of 27, 25, and 121 Gg for $PM_{10}$, $NO_x$, and CO as compared to those of 8, 6, and 34 Gg from the energy industry, respectively.

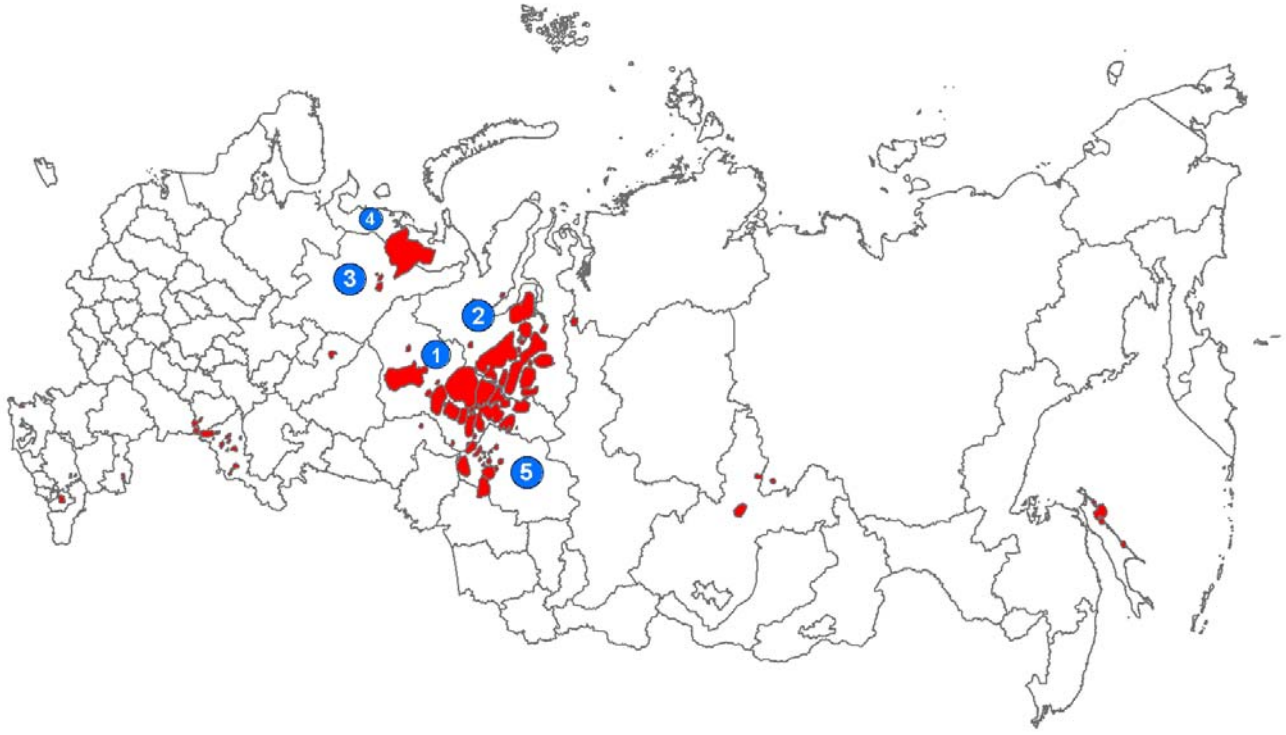


**Fig. 5.** The areas of gas flaring in Russia derived from the U.S. Air Force Defense Meteorological Satellite Program (DMSP) Operational Linescan System (OLS). The five major gas flaring areas are marked in the plot with index from ①–⑤ representing Khanty-Mansiysk, Yamal-Nenets, Komi, Nenets, and Tomsk, respectively.

**Table 2.** Emission factors for gas flaring emission estimation.

| Species | Original Emission Factor ($lb/10^6$ Btu) | Converted Emission Factor ($kg/m^3$)[a] | Mean (± S.D.) Emission Factor ($kg/m^3$) |
|---|---|---|---|
| PM[b] | 0.0, 0.027, 0.12, 0.19 | 0, 0.001, 0.0045, 0.0071 | 0.0032 ± 0.0033 |
| CO[c] | 0.28–0.55 | 0.010–0.02 | 0.015 ± 0.007 |
| $NO_x$[c] | 0.049–0.14 | 0.0018–0.0052 | 0.0035 ± 0.0024 |

[a] Emission factors are converted based on a fuel heating value of 87 $MJ/m^3$ (1 Btu = 1055.06 J).
[b] Calculated from the soot concentrations using F-factor method on a dry basis, assuming 3% $O_2$ in exhaust (RTI, 2011). Four different soot concentrations in flare: non-smoking flares, 0 μg/L; lightly smoking flares, 40 μg/L; average smoking flares, 177 μg/L; and heavily smoking flares, 274 μg/L (U.S. Environmental Protection Agency, 1995).
[c] TCEQ (Texas Commission on Environmental Quality) 2008 Emissions Inventory Guidelines (TCEQ, 2009).

**Table 3.** 2008 gas flaring emission for PM, $NO_x$, and CO in five major flaring regions and the whole Russian Federation. Uncertainties of estimated emission (one standard deviation) are shown in the parentheses.

| Russian Regions | | Flaring Emission (Gg) | | |
|---|---|---|---|---|
| Index (Fig. 5) | Name | PM | CO | $NO_x$ |
| ① | Khanty-Mansiy | 63.08 (65.37) | 286.5 (87.22) | 60.11 (30.46) |
| ② | Yamal-Nenets | 26.59 (27.55) | 120.76 (36.76) | 25.34 (12.84) |
| ③ | Komi | 11.80 (12.23) | 53.60 (16.32) | 11.25 (5.70) |
| ④ | Nenets | 11.23 (11.64) | 51.00 (15.52) | 10.70 (5.42) |
| ⑤ | Tomsk | 6.68 (6.92) | 30.32 (9.23) | 6.36 (3.22) |
| Russian Federation | | 132.39 (137.20) | 601.29 (183.04) | 126.15 (63.92) |

The large $NO_x$ emission from flaring should also partly account for the observed $NO_2$ columns from satellite in the flaring source regions. As shown in Fig. 3(b), high $NO_2$ columns spread over the central and southern parts of Yamalo-Nenets where less or even no power plants located there. This could be explained by the intense flaring emissions there. Fig. 5 demonstrates that the flaring source region in Yamalo-Nenets corresponded relatively well to the high $NO_2$ columns there. The Nenets Autonomous Okrug is another example demonstrating the possible impact of flaring emission on the air pollutant levels. As shown in Fig. 3(a), there were two power plants in this region while neither of them located in the high $NO_2$ column zone. As we compare the flaring source area in Nenets to the spatial distribution of $NO_2$, it showed relatively good consistency between them.

### *Emissions from Mining Activities*

In addition to the underestimated emission from power plants and the missing emission from gas flaring as discussed in the previous two sections, emission produced during mining processes could be another potential source that is neglected or underestimated in RUS_EDGAR. Russia is one of the world's leading mineral producing countries. The mineral raw material sector in Russia, which included mineral extraction and processing, produced about 30% of the country's gross domestic product (GDP) (USGS, 2007). The national mining emission from RUS_FSSS reached 275, 151 and 2229 Gg for $PM_{10}$, $NO_x$, and CO, respectively (Table 1). However, in RUS_EDGAR, the mining emissions for the above three species were much lower to be 19, 47, and 379 Gg for $PM_{10}$, $NO_x$, and CO, respectively. Thus, RUS_EDGAR underestimated mining emissions by a factor of ~16, 2, and 4 for $PM_{10}$, $NO_x$, and CO, respectively, as compared to RUS_FSSS.

In order to find out which part of Russia had the biggest discrepancy for mining emissions between the two inventories, we distributed the total Russian mining emission to the provincial level by using the provincial economic revenues from mining and quarrying as a proxy (method described in Section 2.1.2). Fig. 6 shows the ratio of RUS_FSSS vs. RUS_EDGAR in the mining emission sector for $PM_{10}$, $NO_x$, and CO at the Russian provincial level, respectively. The ratios above and below 1.0 are indicated by different colors. It is found that the regions with ratios less than 1.0 (means RUS_FSSS is lower than RUS_EDGAR) mainly distributed in areas with higher human population density (Fig. 1), e.g., the European and southern parts of Russia. While most underestimations of mining emission occurred in the remote areas, e.g., the Urals, Siberia, the Far East, and parts of the Northwestern Federal District. Of which, Khanty-Mansiysk and Nenets were again among the most underestimated regions. A factor of over 1000 lower in RUS_EDGAR was indicated in the figure for the $PM_{10}$ and CO mining emission. In some other regions, e.g., Yamalo-Nenets, Sakha, Evenk, and Chukotka, where mining activities were active, their mining emissions were also underestimated significantly.

## OUTLOOK

Based on the results presented above, the regions identified with most considerable emissions missing were all located at high latitudes, e.g., Khanty-Mansiysk, Yamal-Nenets, Nenets, and Chukotka (Figs. 3 and 5). Fig. S3 ((Cheng, 2013), unpublished plot from the same project) plots the probabilities of emission source regions by using the Potential Source Contribution Function (PSCF) and measurement data of black carbon at Tiski Bay in 2010.

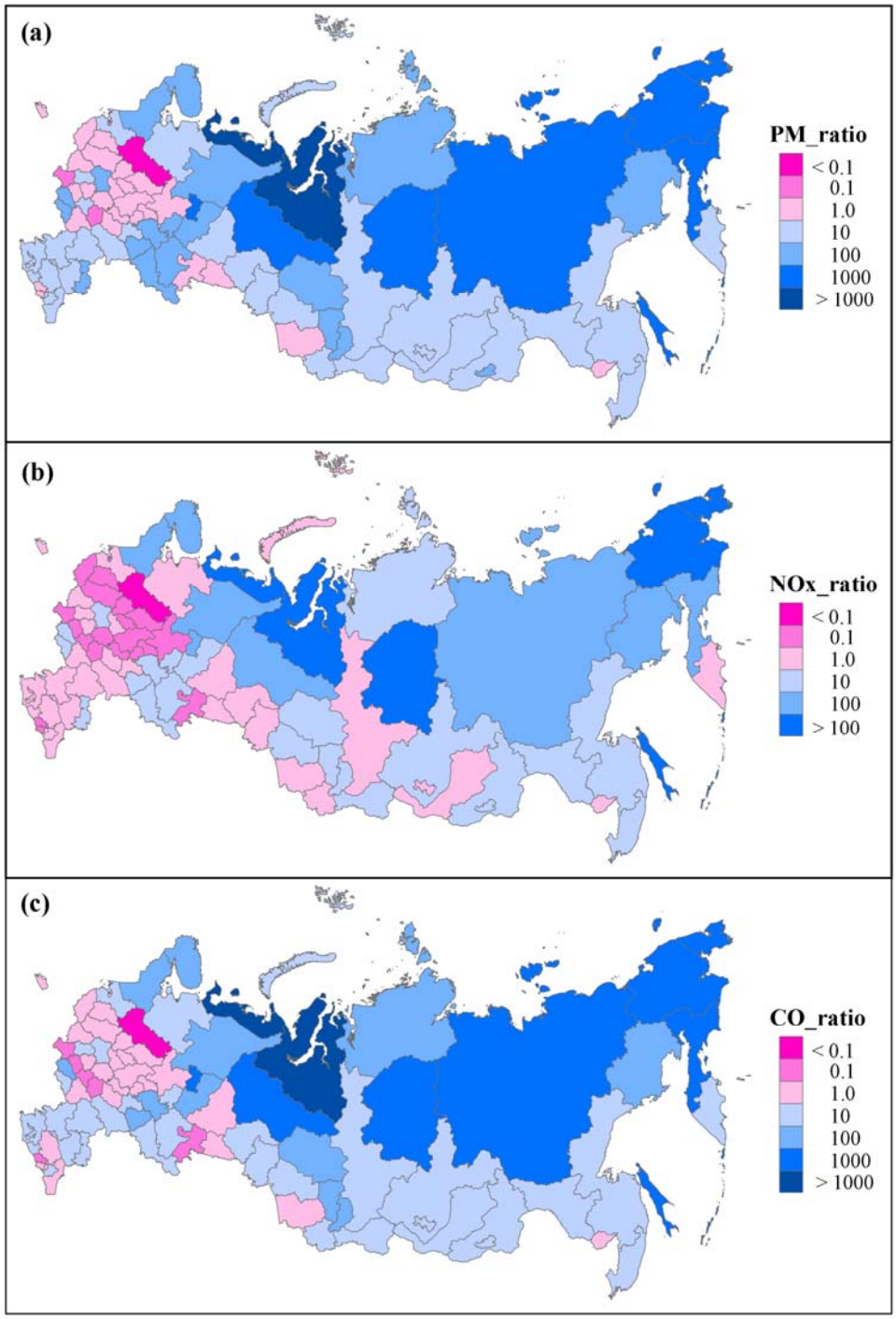


**Fig. 6.** The ratio of RUS_FSSS vs. RUS_EDGAR in the mining emission sector for (a) PM, (b) $NO_x$, and (c) CO at the Russian provincial level.

Hot spots were evident in Urals, central part and eastern tip of Russia, corroborating well with our results above. Thus, if by using EDGAR as the model input, the impact from Russian continental anthropogenic emissions on the Arctic could be possibly underestimated. The addition of the significant Russian emissions identified in this study might shift the view of the source apportionment of the Arctic pollution and will be especially important for the impact assessment of long-range transported pollutants on air quality and climate change in the Arctic region. It is important to note that there may be other significantly under-reported emissions, such as industrial, residential and/or transportation emissions. An up-to-date and comprehensive Russian emission inventory requires close collaboration with local authorities. Detailed local information of fuel usage, emission factors, and efficiencies dependent on economic sectors and regions and are necessary. Currently, we are working on the speciation of total PM emissions with spatial/temporal

allocation and will further implement the newly constructed Russian emissions into multiple 3-D models. It is expected that the improved Russian emissions will significantly advance the simulation of air pollutants and climatic impacts over the Arctic region. This study and our future works will also provide insights on how emission controls should be targeted to alleviate the climate change over the Arctic.

## CONCLUSIONS

In this study, our aim was to elucidate the differences between the Russian part of the global emission inventory EDGAR and a Russian federal emission inventory. From the view of the GEOS-Chem modeling, AOD at multi-AERONET sites in Russia were underestimated by about 150%–300%, indicating a significant underestimation of Russian local emissions. Three emission sectors including fossil-fuel fired power plants, gas flaring and mining emissions were specifically investigated. Considerable fossil-fuel fired power plants were found missing in RUS_EDGAR in comparison to CARMA and the spatial pattern of $NO_2$ columns observed from OMI. Most missing power plants were found in the Urals Federal District and the Chukotka Autonomous Okrug. The total underestimated energy production in EDGAR reached $6.18 \times 10^7$ MWh, accounting for about 9.6% of the total energy production in Russia. In comparison to a Russian federal emission inventory (RUS_FSSS), around 70% of the Russian provinces showed lower $NO_x$ and $PM_{10}$ emission in EDGAR. The total $NO_x$ and $PM_{10}$ emission in RUS_FSSS reached 3419 and 801 Gg, compared to that of 2267 and 382 Gg in RUS_EDGAR, respectively. Emissions from the Khanty-Mansiysk, Yamalo-Nenets, and Chukotka Autonomous Okrugs had the largest discrepancies between RUS_EDGAR and RUS_FSSS.

Russia's gas flaring combustion was another emission source that was neglected in RUS_EDGAR although Russia is the world's largest gas flaring country. Its national PM, $NO_x$, and CO emission from gas flaring reached 132, 126, and 601 Gg in 2008, respectively. The Urals Federal District and the Northwestern Federal District are Russia's main oil and gas producing bases and also the major gas flaring regions. Khanty-Mansiysk Autonomous Okrug, Yamalo-Nenets Autonomous Okrug, Komi Republic, Nenets Autonomous Okrug, and Tomsk Oblast were the five largest gas flaring areas in Russia. The gas flaring emissions of PM, $NO_x$ and CO in those regions were estimated to overwhelm the other emission sources. And it could partly explain the widespread high $NO_2$ columns detected by OMI where there were no or very few power plants.

Lastly, Russia's mining emissions in RUS_EDGAR were also found significantly underestimated with a factor of ~16, 2, and 4 lower for $PM_{10}$, $NO_x$, and CO, respectively, as compared to RUS_FSSS. The largest underestimated emissions occurred in remote areas, e.g., the Urals, Siberia, the Far East, and parts of the Northwestern Federal District.

## ACKNOWLEDGMENTS

This work is supported by Interagency Acquisition Agreement S-OES-11_IAA-0027 from the U.S. Department of State to the U.S. Department of Energy. Meng-Dawn Cheng, John M. Storey, and Vitaly Y. Prikhodko were supported by the U.S. Department of Energy Office of Policy and International Affairs, and performed at Oak Ridge National Laboratory (ORNL). ORNL is managed by UT-Battelle, LLC, for the U.S. Department of Energy under contract DE-AC05-00OR22725. This work does not reflect the official views or policies of the United States Government or any agency thereof, including the funding entities. The mention of any computer software, data products, and or computational hardware does not represent endorsement by the authors nor organizations that the authors are associated with.

## SUPPLEMENTARY MATERIALS

Supplementary data associated with this article can be found in the online version at http://www.aaqr.org.

## REFERENCES

Andreae, M.O. and Merlet, P. (2001). Emission of Trace Gases and Aerosols from Biomass Burning. *Global Biogeochem. Cycles* 15: 955–966.

Cheng, M.D. (2014). Geolocating Russian Sources for Arctic Black Carbon. *Atmos. Environ.* 92: 398–410.

EDGAR (2011). Main Differences between EDGAR Version 4.2 and 4.1. http://edgar.jrc.ec.europa.eu/Main_differences_between_EDGARv42_and_v41.pdf.

EDGAR (2013). http://edgar.jrc.ec.europa.eu/methodology.php.

EEA (European Environment Agency) (2013). EMEP/EEA Air Pollutant Emission Inventory Guidebook 2013, Part B: Sectoral Guidance Chapters: 1.A.1 Energy Industries, Published on Aug 29, 2013.

EIA (U.S. Energy Information Administration) (2013). Russia Electricity Net Generation (1992-2011), Data Last Updated on May 30, 2013.

Eleftheriadis, K., Vratolis, S. and Nyeki, S. (2009). Aerosol Black Carbon in the European Arctic: Measurements at Zeppelin Station, Ny-Alesund, Svalbard from 1998-2007. *Geophys. Res. Lett.* 36, doi: 10.1029/2008GL035741.

Elvidge, C.D., Ziskin, D., Baugh, K.E., Tuttle, B.T., Ghosh, T., Pack, D.W., Erwin, E.H. and Zhizhin, M. (2009). A Fifteen Year Record of Global Natural Gas Flaring Derived from Satellite Data. *Energies* 2: 595–622.

Fisher, J.A., Jacob, D.J., Purdy, M.T., Kopacz, M., Le Sager, P., Carouge, C., Holmes, C.D., Yantosca, R.M., Batchelor, R.L., Strong, K., Diskin, G.S., Fuelberg, H.E., Holloway, J.S., Hyer, E.J., McMillan, W.W., Warner, J., Streets, D.G., Zhang, Q., Wang, Y. and Wu, S. (2010). Source Attribution and Interannual Variability of Arctic Pollution in Spring Constrained by Aircraft (ARCTAS, ARCPAC) and Satellite (AIRS) Observations of Carbon Monoxide. *Atmos. Chem. Phys.* 10: 977–996, doi: 910.5194/acp-5110-5977-2010.

FNI (Fridtjof Nansen Institute) (2010). Associated Petroleum Gas in Russia: Reasons for Non-utilization, Written by

Tonje Hulbak Røland, ISSN:1504–9744.

FSSS (Federal State Statistics Service) (2011). Russia in Figures: Section 1. Basic Social and Economic Characteristics of the Russian Federation (in Russian), http://www.gks.ru/bgd/regl/b11_12/Main.htm.

Fu, J.S., Hsu, N.C., Gao, Y., Huang, K., Li, C., Lin, N.H. and Tsay, S.C. (2012). Evaluating the Influences of Biomass Burning during 2006 BASE-ASIA: A Regional Chemical Transport Modeling. *Atmos. Chem. Phys.* 12: 3837–3855.

Fu, S.J., Lam, Y.F., Gao, Y., Jacob, J.D., Carouge, C., Corbitt, D.E., Zhang, L. and Fairlie, T.D. (2011). 2006-2008 CMAQ Initial and Boundary Conditions Using GEOS-Chem Simulations, Final Report Submitted to Office Air Quality Planning and Standards (OAQPS), U.S. Environmental Protection Agency.

Harrigan, D.L., Fuelberg, H.E., Simpson, I.J., Blake, D.R., Carmichael, G.R. and Diskin, G.S. (2011). Anthropogenic Emissions during Arctas-A: Mean Transport Characteristics and Regional Case Studies. *Atmos. Chem. Phys.* 11: 8677–8701, doi: 8610.5194/acp-8611-8677-2011.

Hirdman, D., Burkhart, J.F., Sodemann, H., Eckhardt, S., Jefferson, A., Quinn, P.K., Sharma, S., Strom, J. and Stohl, A. (2010a). Long-term Trends of Black Carbon and Sulphate Aerosol in the Arctic: Changes in Atmospheric Transport and Source Region Emissions. *Atmos. Chem. Phys.* 10: 9351–9368, doi:9310.5194/acp-9310-9351-2010.

Hirdman, D., Sodemann, H., Eckhardt, S., Burkhart, J.F., Jefferson, A., Mefford, T., Quinn, P.K., Sharma, S., Strom, J. and Stohl, A. (2010b). Source Identification of Short-lived Air Pollutants in the Arctic Using Statistical Analysis of Measurement Data and Particle Dispersion Model Output. *Atmos. Chem. Phys.* 10: 669–693, doi: 610.5194/acp-5110-5669-2010.

Holben, B.N., Eck, T.F., Slutsker, I., Tanre, D., Buis, J.P., Setzer, A., Vermote, E., Reagan, J.A., Kaufman, Y.J., Nakajima, T., Lavenu, F., Jankowiak, I. and Smirnov, A. (1998). AERONET - A Federated Instrument Network and Data Archive for Aerosol Characterization. *Remote Sens. Environ.* 66: 1–16.

Huang, K., Fu, J.S., Christina Hsu, N., Gao, Y., Dong, X.Y., Tsay, S.C. and Lam, Y.F. (2012). Impact Assessment of Biomass Burning on Air Quality in Southeast and East Asia during BASE-ASIA. *Atmos. Environ.* 78: 291–302, doi: 10.1016/j.atmosenv.2012.1003.1048.

Huang, L., Gong, S.L., Sharma, S., Lavoue, D. and Jia, C.Q. (2010). A Trajectory Analysis of Atmospheric Transport of Black Carbon Aerosols to Canadian High Arctic in Winter and Spring (1990-2005). *Atmos. Chem. Phys.* 10: 5065–5073, doi:5010.5194/acp-5010-5065-2010.

Knizhnikov, A. and Poussenkova, N. (2009). Russian Associated Gas Utilization: Problems and Prospects, Annual review within the framework of the joint project of the Institute of World Economy and International Relations of the Russian Academy of Sciences and WWF-Russia "Environment and Energy. International Context".

Koch, D. and Hansen, J. (2005). Distant Origins of Arctic Black Carbon: A Goddard Institute for Space Studies ModelE Experiment. *J. Geophys. Res.* 110: D04204, doi: 10.1029/2004JD005296.

Koch, D., Schulz, M., Kinne, S., McNaughton, C., Spackman, J.R., Balkanski, Y., Bauer, S., Berntsen, T., Bond, T.C., Boucher, O., Chin, M., Clarke, A., De Luca, N., Dentener, F., Diehl, T., Dubovik, O., Easter, R., Fahey, D.W., Feichter, J., Fillmore, D., Freitag, S., Ghan, S., Ginoux, P., Gong, S., Horowitz, L., Iversen, T., Kirkevag, A., Klimont, Z., Kondo, Y., Krol, M., Liu, X., Miller, R., Montanaro, V., Moteki, N., Myhre, G., Penner, J.E., Perlwitz, J., Pitari, G., Reddy, S., Sahu, L., Sakamoto, H., Schuster, G., Schwarz, J.P., Seland, O., Stier, P., Takegawa, N., Takemura, T., Textor, C., van Aardenne, J.A and. Zhao, Y. (2009). Evaluation of Black Carbon Estimations in Global Aerosol Models. *Atmos. Chem. Phys.* 9: 9001–9026, doi: 9010.5194/acp-9009-9001-2009.

Law, K.S. and Stohl, A. (2007). Arctic Air Pollution: Origins and Impacts. *Science* 315: 1537–1540, doi: 1510.1126/science.1137695.

Li, C., Zhang, Q., Krotkov, N.A., Streets, D.G., He, K.B., Tsay, S.C. and Gleason, J.F. (2010). Recent Large Reduction in Sulfur Dioxide Emissions from Chinese Power Plants Observed by the Ozone Monitoring Instrument. *Geophys. Res. Lett.* 37, doi: 10.1029/2010 GL042594.

Lin, J.T. (2012). Satellite Constraint for Emissions of Nitrogen Oxides from Anthropogenic, Lightning and Soil Sources over East China on a High-resolution Grid. *Atmos. Chem. Phys.* 12: 2881–2898.

Makarova, M.V., Ionov, D.V., Rakitin, A.V. and Orlov, A.V. (2011). Characterizing the Impact of Urban Sources in Russia on Air Pollution in northern Europe, Presented at the 10th Annual CMAS Conference, Chapel Hill, NC, October 24–26, 2011.

Mu, M., Randerson, J.T., van der Werf, G.R., Giglio, L., Kasibhatla, P., Morton, D., Collatz, G.J., DeFries, R.S., Hyer, E.J., Prins, E.M., Griffith, D.W.T., Wunch, D., Toon, G.C., Sherlock, V. and Wennberg, P.O. (2010). Daily and 3-hourly Variability in Global Fire Emissions and Consequences for Atmospheric Model Predictions of Carbon Monoxide. *J. Geophys. Res.* 116: D24303, doi: 10.1029/2011JD016245.

NOAA (National Geophysical Data Center) (2011). Global Gas Flaring Estimates - Global/Country Results 1994-2010, http://www.ngdc.noaa.gov/dmsp/interest/gas_flares.html.

RTI International (2011). Emission Estimation Protocol for Petroleum Refineries, submitted to OAQPS, U.S. EPA.

Sharma, S., Andrews, E., Barrie, L.A., Ogren, J.A. and Lavoue, D. (2006). Variations and Sources of the Equivalent Black Carbon in the High Arctic Revealed by Long-term Observations at Alert and Barrow: 1989-2003. *J. Geophys. Res.* 111: D14208, doi: 10.1029/2005 JD006581.

Shindell, D.T., Chin, M., Dentener, F., Doherty, R.M., Faluvegi, G., Fiore, A.M., Hess, P., Koch, D.M., MacKenzie, I.A., Sanderson, M.G., Schultz, M.G., Schulz, M., Stevenson, D.S., Teich, H., Textor, C., Wild, O., Bergmann, D.J., Bey, I., Bian, H., Cuvelier, C., Duncan,

B.N., Folberth, G., Horowitz, L.W., Jonson, J., Kaminski, J.W., Marmer, E., Park, R., Pringle, K.J., Schroeder, S., Szopa, S., Takemura, T., Zeng, G., Keating, T.J. and Zuber, A. (2008). A Multi-model Assessment of Pollution Transport to the Arctic. *Atmos. Chem. Phys.* 8: 5353–5372, doi:5310.5194/acp-5358-5353-2008.

SRI Atmosphere (2012). Methodologies for the Calculation, Regulation and Control of Emissions into the air (http://www.nii-atmosphere.ru/?article=17).

Stohl, A. (2006). Characteristics of Atmospheric Transport into the Arctic Troposphere. *J. Geophys. Res.* 111: D11306, doi: 10.1029/2005JD006888.

Stohl, A., Klimont, Z., Eckhardt, S., Kupiainen, K., Shevchenko, V.P., Kopeikin, V.M. and Novigatsky, A.N. (2013). Black Carbon in the Arctic: The Underestimated Role of Gas Flaring and Residential Combustion Emissions. *J. Geophys. Res.* 13: 8833–8855, doi: 10.5194/acp-13-8833-2013.

USGS (U.S. Geological Survey) (2007). Mineral Year Book – The Mineral Industry of Russia, by Richard M. Levine, Mark Brininstool, and Glenn J. Wallace, http://minerals.usgs.gov/minerals/pubs/country/2007myb3-2007-rs.pdf.

van der Werf, G. R., Randerson, J.T., Giglio, L., Collatz, G. J., Mu, M., Kasibhatla, P.S., Morton, D.C., DeFries, R. S., Jin, Y. and van Leeuwen, T.T. (2010). Global Fire Emissions and the Contribution of Deforestation, Savanna, Forest, Agricultural, and Peat Fires (1997–2009). *Atmos. Chem. Phys.* 10: 11707–11735, doi: 10.5194/acp-10-11707-2010.

Wang, Q., Jacob, D.J., Fisher, J.A., Mao, J., Leibensperger, E.M., Carouge, C.C., Le Sager, P., Kondo, Y., Jimenez, J.L., Cubison, M.J. and Doherty, S.J. (2011). Sources of Carbonaceous Aerosols and Deposited Black Carbon in the Arctic in Winter-spring: Implications for Radiative Forcing. *Atmos. Chem. Phys.* 11: 12453–12473, doi: 10.5194/acp-11-12453-2011.

Wheeler, D. and Ummel, K. (2008). Calculating CARMA: Global Estimation of $CO_2$ Emissions from the Power Sector. Center for Global Development, Working Paper 145.

World Bank (2012). Estimated Flared Volumes from Satellite Data, 2006-2010. http://web.worldbank.org/WBSITE/EXTERNAL/TOPICS/EXTOGMC/EXTGGFR/0,,contentMDK:22137498~pagePK:64168445~piPK:64168309~theSitePK:578069,00.html.

Zhang, L., Jacob, D.J., Knipping, E.M., Kumar, N., Munger, J.W., Carouge, C.C., van Donkelaar, A., Wang, Y.X. and Chen, D. (2012). Nitrogen Deposition to the United States: Distribution, Sources, and Processes. *Atmos. Chem. Phys.* 12:4539–4554, doi: 10.5194/acp-12-4539-2012.

Zhang, Q., Streets, D.G. and He, K.B. (2009). Satellite Observations of Recent Power Plant Construction in Inner Mongolia, China. *Geophys. Res. Lett.* 36: L15809, doi: 10.1029/2009GL038984.

*Received for review, August 12, 2014*
*Accepted, October 31, 2014*

# Supplementary information

## Identification of missing anthropogenic emission sources in Russia: implication for modeling Arctic haze

**Kan Huang[1], Joshua S. Fu[1*], Elke L. Hodson[2,†], Xinyi Dong[1], Joe Cresko[2], Vitaly Y. Prikhodko[3], John M. Storey[3], Meng-Dawn Cheng[3]**

*[1] Department of Civil and Environmental Engineering, The University of Tennessee, Knoxville, TN 37996, USA*
*[2] U.S. Department of Energy, Washington, DC, USA*
*[3] Energy and Environmental Sciences Directorate, Oak Ridge National Laboratory, Oak Ridge, TN, USA*
*[†] Oak Ridge Institute for Science and Education Fellow*

[*] Corresponding author. Tel: 1-865-974-2503; Fax: 1-865-974-2669
E-*mail address*: jsfu@utk.edu

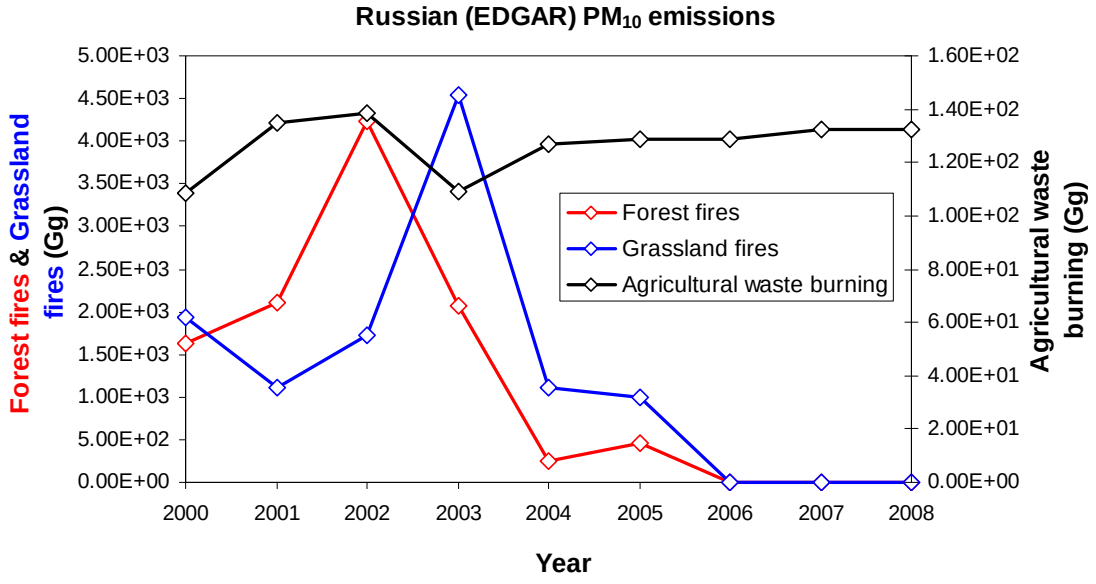


**Fig. S1.** Annual $PM_{10}$ emissions (2000 – 2008) of Russia in three sectors that are relevant to biomass burning, i.e. agricultural waste burning, forest fires, and grassland fires.

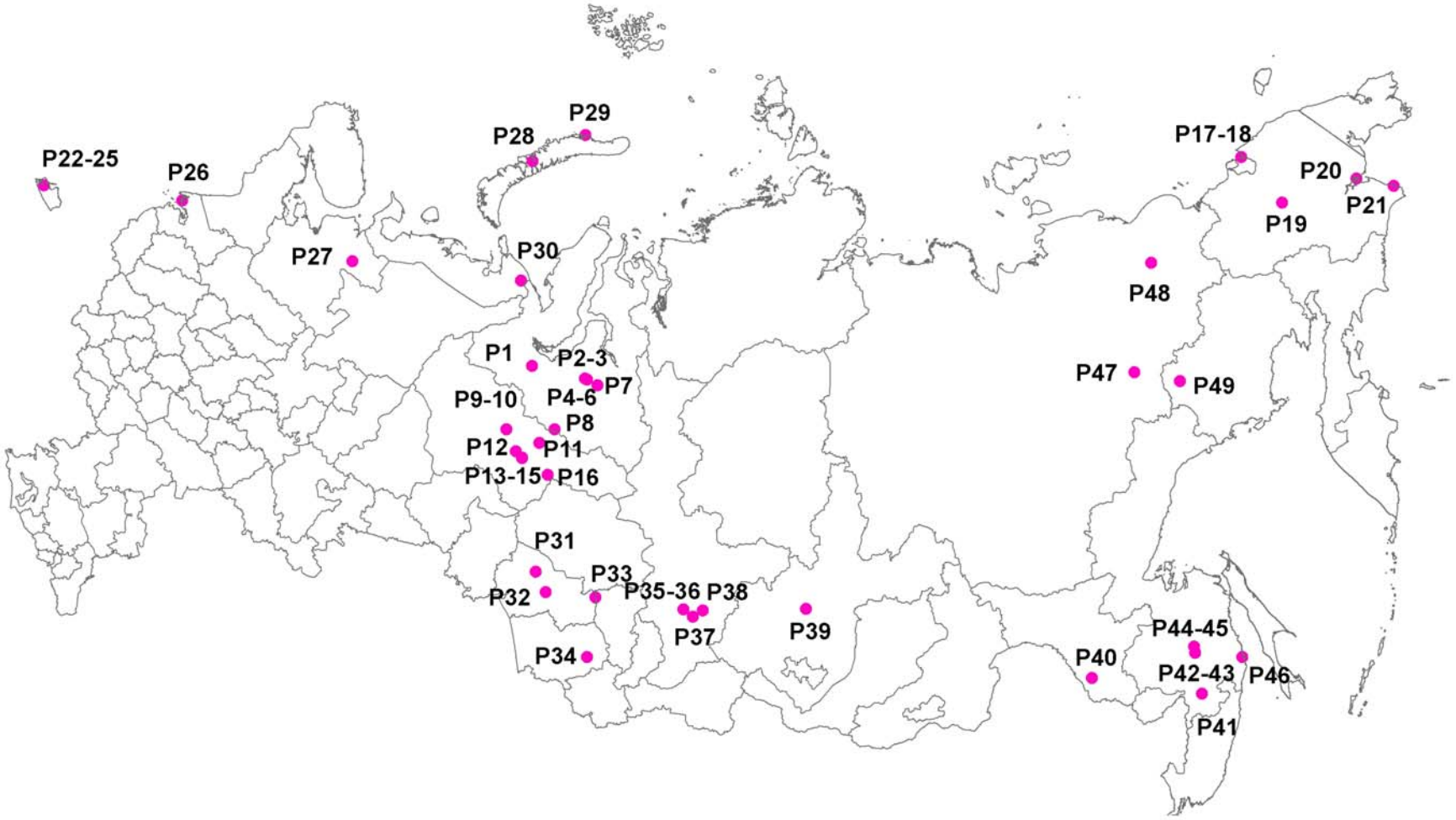


**Fig. S2.** Locations of missing power plants in the EDGAR emission inventory as compared to CARMA. Corresponding information of each power plant is listed in Table S1.

**Description of Potential source contribution function**

The PSCF is a technique for source region identification that requires both ambient air chemistry data and backward air mass trajectory. PSCF analysis yields a two-dimensional map that shows a synthetic probability field describing the source strength of a geographical area (i.e., a grid cell), which is called as the "Potential Source Contribution". The total numbers ($n_{i,j}$) of trajectory endpoints (i.e. coordinates of the back trajectory for each hour before arriving at the receptor site) falling within grid cell [$i$,$j$] during the study period are counted. Also, the number of those in the same grid cell with pollutant level higher than a set threshold was calculated as $m_{i,j}$. Then, the ratio between $n_{i,j}$ and $m_{i,j}$ is the PSCF value for this grid cell: $PSCF_{i,j} = m_{i,j}/n_{i,j}$. To minimize the biased PSCF caused by the low $n_{i,j}$ values, $PSCF_{ij}$ was weighted with $w_{ij}$ by setting at 0.1 for $n_{i,j} < 9$, and 1.0 for $n_{i,j} \geq 10$. Note that PSCF didn't incorporate any emission input and couldn't resolve detailed small-scale features while it was an indication of the likelihood that a given region contributed to the receptor site.

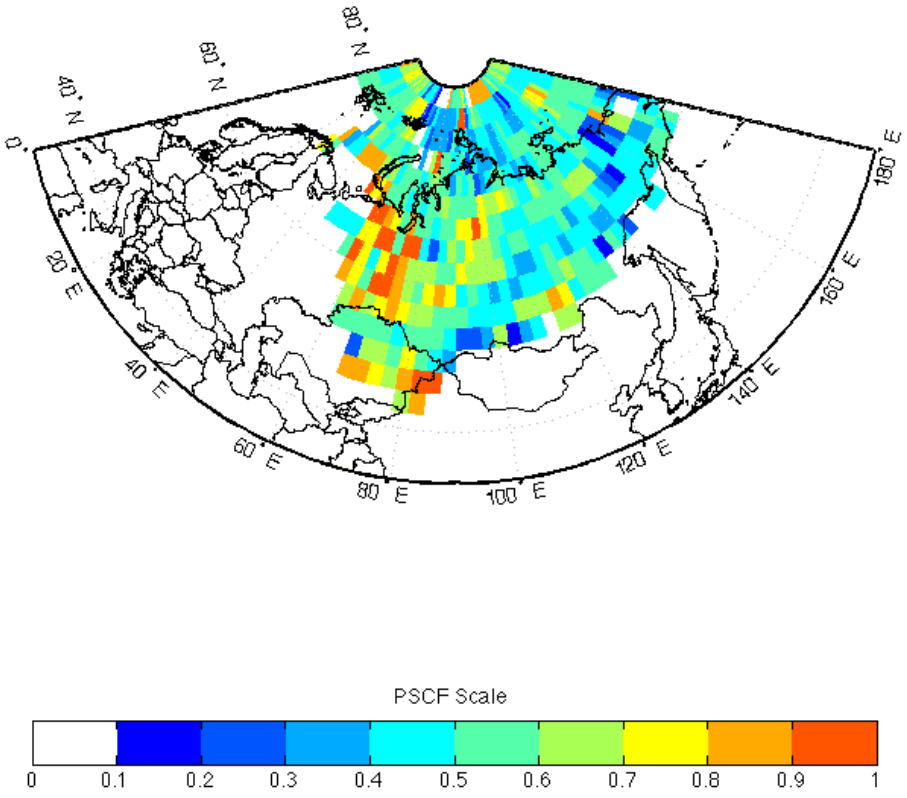


**Fig. S3.** Potential source contribution function (PSCF) probability map for black carbon measurement at Tiski (71.6° N, 128.9° E) during the autumn in 2010.

**Table S1.** Name, energy capacity, and locations of missing power plants as indicated in Figure S3.

| Index | Power Plant Name | Energy_2007(MWh) | State | Latitude | Longitude |
|---|---|---|---|---|---|
| P1 | Urengoy | 167860 | Yamal-Nenets | 65.63 | 70.26 |
| P2 | NOVY URENGOI | 35870 | Yamal-Nenets | 66.08 | 76.63 |
| P3 | NOVY URENGOI-2 | 148740 | Yamal-Nenets | 66.08 | 76.63 |
| P4 | TARASOVSKOYE FIELD | 546830 | Yamal-Nenets | 66.07 | 76.93 |
| P5 | SEVERO-GUBKINSKY | 94616 | Yamal-Nenets | 66.07 | 76.93 |
| P6 | HASIREYSK FIELD | 237540 | Yamal-Nenets | 66.07 | 76.93 |
| P7 | URENGOYSK | 167860 | Yamal-Nenets | 65.97 | 78.37 |
| P8 | NOYABRSK | 831010 | Yamal-Nenets | 63.20 | 75.45 |
| P9 | WEST SALYMN FIELD | 300500 | Khanty-mansiy | 62.23 | 70.64 |
| P10 | SEVERO-LABATYUGANSKOYE | 159700 | Khanty-mansiy | 62.23 | 70.64 |
| P11 | VATYEGANSKOYE FIELD | 756860 | Khanty-Mansiy | 62.27 | 74.48 |
| P12 | LYANTOR CITY HOSPITAL | 58 | Khanty-Mansiy | 61.42 | 72.52 |
| P13 | SURGUT-2 | 15600000 | Khanty-Mansiy | 61.24 | 73.40 |
| P14 | SURGUT MUNICIPAL HOSPITAL | 350 | Khanty-Mansiy | 61.25 | 73.42 |
| P15 | SURGUT ADMIN HQ | 109 | Khanty-Mansiy | 61.25 | 73.42 |
| P16 | NIZHNEVARTOVSK | 6707400 | Khanty-Mansiy | 60.93 | 76.55 |
| P17 | CHAUNSK | 152617 | Chukotka | 69.70 | 170.31 |
| P18 | PEVEK DES | 1755 | Chukotka | 69.70 | 170.31 |
| P19 | KUPOL MINE | 88558 | Chukotka | 66.78 | 169.55 |
| P20 | ANADYR | 360102 | Chukotka | 64.75 | 177.48 |
| P21 | BERINGOVSKIY | 4416 | Chukotka | 63.05 | 179.32 |
| P22 | KALININGRAD MILL | 997594 | Kaliningrad | 54.71 | 20.50 |
| P23 | KALININGRAD-02 CHPP | 1314420 | Kaliningrad | 54.71 | 20.50 |
| P24 | KALININGRAD-05 | 166380 | Kaliningrad | 54.71 | 20.50 |
| P25 | KALININGRAD GT PLANT | 22388 | Kaliningrad | 54.71 | 20.50 |
| P26 | SEVERO-ZAPADNAYA | 2560327 | Saint Petersburg | 60.37 | 28.60 |
| P27 | LESHUKONSKAYA DES | 2196 | Arkhangel'sk | 64.90 | 45.77 |
| P28 | NOVAYA ZEMLYA | 18285 | Arkhangelskaya | 74.00 | 56.00 |
| P29 | VELSKAYA | 212830 | Arkhangelskaya | 76.23 | 60.99 |
| P30 | VARANDEY TERMINAL | 336380 | Arkhangelskaya | 69.05 | 64.00 |
| P31 | SURGUT-1 | 14827000 | Novosibirskaya | 56.06 | 78.72 |
| P32 | VERKH-TARSKOYE FIELD | 55114 | Novosibirskaya | 55.22 | 80.14 |
| P33 | YURGINSKAYA | 262340 | Kemerovskaya | 55.69 | 84.64 |
| P34 | BIYSK-1 | 3778294 | Biysk | 52.57 | 85.25 |
| P35 | KRASNOYARSK-1 | 1948200 | Krasnoyarskiy Kray | 56.01 | 92.79 |
| P36 | KRASNOYARSK-2 | 1194700 | Krasnoyarskiy Kray | 56.01 | 92.79 |
| P37 | SHAPINSKOE GAS PLANT | 96652 | Krasnoyarskiy Kray | 55.72 | 93.76 |
| P38 | KRASNOYARSK-2 SDPP | 3519000 | Krasnoyarskiy Kray | 56.11 | 94.59 |
| P39 | IRKUTSK-16 | 106755 | Irkutsk | 56.57 | 104.12 |
| P40 | LUKIANOVKA | 3067 | Amurskaya | 50.83 | 128.20 |
| P41 | MUKHEN | 24148 | Khabarovsk Krai | 48.10 | 136.10 |
| P42 | KHABAROVSK-1 | 1035700 | Khabarovsk Krai | 50.23 | 136.90 |
| P43 | AMUR-1 | 1029500 | Khabarovsk Krai | 50.23 | 136.90 |
| P44 | KOMSOMOLSK-2 | 1321400 | Khabarovsk Krai | 50.55 | 137.02 |
| P45 | KOMSOMOLSK-3 | 1359900 | Khabarovsk Krai | 50.55 | 137.02 |
| P46 | MAYSKIY | 390060 | Khabarovsk Krai | 49.00 | 140.21 |
| P47 | INDIGIRSKA | 14291 | Sakha | 64.57 | 143.20 |
| P48 | ALEKO-KYUEL | 95 | Sakha | 68.70 | 151.90 |
| P49 | ARKAGALA | 1190100 | Magadanskaya | 63.05 | 147.19 |